

The ground state in a proximity to a possible Kitaev spin liquid:

An undistorted honeycomb iridate Na_xIrO_3 ($0.60 \leq x \leq 0.80$)

Hengdi Zhao¹, Bing Hu^{1,2}, Feng Ye³, Minhyea Lee¹, Pedro Schlottmann⁴ and Gang Cao^{1*}

¹*Department of Physics, University of Colorado at Boulder, Boulder, Colorado 80309, USA*

²*School of Mathematics and Physics, North China Electric Power University, Beijing 102206, China*

³*Neutron Scattering Division, Oak Ridge National Laboratory, Oak Ridge, TN 37831, USA*

⁴*Department of Physics, Florida State University, Tallahassee, FL 32306, USA*

We report results of our study of a newly synthesized honeycomb iridate Na_xIrO_3 ($0.60 \leq x \leq 0.80$). Single-crystal Na_xIrO_3 adopts a honeycomb lattice noticeably without distortions and stacking disorder inherently existent in its sister compound Na_2IrO_3 . The oxidation state of the Ir ion is a mixed valence state resulting from a majority $\text{Ir}^{5+}(5d^4)$ ion and a minority $\text{Ir}^{6+}(5d^3)$ ion. Na_xIrO_3 is a Mott insulator likely with a predominant pseudospin = 1 state. It exhibits an effective moment of $1.1 \mu_B/\text{Ir}$ and a Curie-Weiss temperature of -19 K but with no discernable long-range order above 1 K. The physical behavior below 1 K features two prominent anomalies at $T_h = 0.9$ K and $T_l = 0.12$ K in both the heat capacity and AC magnetic susceptibility. Intermediate between T_h and T_l lies a pronounced temperature linearity of the heat capacity with a large slope of 77 mJ/mole K^2 , a feature expected for highly correlated metals but not at all for insulators. These results along with comparison drawn with the honeycomb lattices Na_2IrO_3 and $(\text{Na}_{0.2}\text{Li}_{0.8})_2\text{IrO}_3$ point to an exotic ground state in a proximity to a possible Kitaev spin liquid.

*gang.cao@colorado.edu

Introduction Honeycomb lattices with strong spin-orbit interactions (SOI) have been extensively sought and studied because they are most desirable as possible realization of the exactly solvable spin liquid model developed by Kitaev [1]. The honeycomb lattices feature MO_6 ($\text{M} = \text{Ir}$ or Ru) octahedra that are edge-sharing with 90° M-O-M bonds. The magnetic exchange is anisotropically bond-dependent. When individual spins at the sites of a honeycomb lattice are restricted to align along any one of the three bond directions, the Kitaev model predicts a quantum spin-liquid ground state. This novel state hosts short-range correlations and the spin degrees of freedom that fractionalize into Majorana fermions in static Z_2 gauge fields. Theoretical treatments of the honeycomb lattices Na_2IrO_3 and Li_2IrO_3 (including β and γ phases) and more recently $\alpha\text{-RuCl}_3$ [e.g., 2-8] have inspired a large body of experimental work that anticipates the Kitaev physics [e.g., 9-30]. Although strongly frustrated, all these honeycomb lattices are antiferromagnetically ordered with the Néel temperature ranging from 7 K to 18 K. There has been no clear-cut materials realization of a quantum spin liquid (QSL) at ambient conditions thus far.

The absence of a QSL in these honeycomb lattices indicates that the Heisenberg interaction, which competes with the strong Kitaev interaction, is still consequential in the Kitaev-Heisenberg model [25], in part because of stacking disorder and distortions often characterized by unequal M-M bonds inherently existent in these honeycomb lattices [12, 15, 25-30]. This is an experimental challenge that is particularly daunting for honeycomb lattices with strong SOI that renders an extraordinary susceptibility of the ground state to the lattice degrees of freedom [31, 32].

The overwhelming balance of interest has been devoted to the honeycomb lattices hosting five d -electrons and a pseudospin = $1/2$ state, such as Na_2IrO_3 , Li_2IrO_3 and $\alpha\text{-RuCl}_3$, as quantum fluctuations in a QSL with a pseudospin = $1/2$ state are more resilient to classical effects. Honeycomb lattices with a higher spin state, such as the ruthenates Na_2RuO_3 and Li_2RuO_3 with a

$\text{Ru}^{4+}(4d^4)$ ion and a spin = 1 state [33], have remained largely unexplored. It is encouraging that a recent study extends the search of QSLs to honeycomb materials with $S = 3/2$ that show a two-peak characteristic in the heat capacity, a promising sign of a QSL [34].

Here we report structural and physical properties of our newly synthesized single crystals of Na_xIrO_3 ($0.60 \leq x \leq 0.80$). One outstanding feature of this new compound is that Na_xIrO_3 adopts an undistorted honeycomb lattice without stacking disorder or intermixing of Na and Ir inherently existent in its sister compound Na_2IrO_3 [12]. Our chemical and structural analysis indicates that the oxidation state of the Ir ion is a mixed valence state resulting from a majority $\text{Ir}^{5+}(5d^4)$ ion and a minority $\text{Ir}^{6+}(5d^3)$ ion. The insulating Na_xIrO_3 shows an effective moment of $1.1 \mu_B/\text{Ir}$, too large for an anticipated singlet ground state for a strong SOI limit, suggesting a predominant pseudospin = 1 state. It exhibits a Curie-Weiss temperature of -19 K with no discernable long-range order above 1 K. The physical behavior below 1 K presents two prominent anomalies at $T_h = 0.9$ K and $T_l = 0.12$ K, respectively, in both the heat capacity and AC magnetic susceptibility. Intermediate between T_h and T_l lies a pronounced temperature linearity of the heat capacity with an unexpectedly large slope of 77 mJ/mole K^2 , a feature expected for highly correlated metals but not at all for any insulators. These results along with comparison drawn with Na_2IrO_3 and $(\text{Na}_{0.2}\text{Li}_{0.8})_2\text{IrO}_3$ point out an exotic ground state that hosts strong quantum fluctuations likely coexisting with a short-range spin order. Note that the ground state of Na_xIrO_3 is insensitive to x .

Crystal structure The crystal structure of the single crystal Na_xIrO_3 was determined independently using a Bruker D8 Quest ECO single-crystal diffractometer at the University of Colorado Boulder and a Rigaku XtaLAB PRO diffractometer at the Oak Ridge National Laboratory after thorough examinations of dozens of single crystal Na_xIrO_3 . All datasets were refined by using APEX3 and/or SHELXL-2014 program [35] (see Ref. 36 for more details). Single crystal Na_xIrO_3 with x ranging

between 0.60 and 0.80 adopts a quasi-two-dimensional hexagonal structure with space group $P-31m$ (No. 162) (**Fig.1**). There are two distinct Na sites, Na1 and Na2 (**Figs.1a-b**). The Na1 site resides at the center of the honeycomb ring in the ab or honeycomb plane whereas the Na2 site exists between the honeycomb planes. Almost all Na vacancies occur at the Na1 sites within the honeycomb rings whereas the Na2 sites are fully or nearly fully occupied (**Figs.1a-b**); this explains that x in Na_xIrO_3 is hardly smaller than 0.50. Most importantly, the edge-sharing IrO_6 octahedra form a robust, *undistorted* honeycomb lattice characterized by an exactly equal Ir-Ir bond distance, $d_{\text{Ir-Ir}}$, between all neighboring Ir atoms (**Fig.1c**), independent of the Na1 deficiency [36]. The Ir sites are fully or nearly fully occupied, and there is no discernable oxygen deficiency. The characteristic of the honeycomb lattice is also evident in both the X-ray diffraction pattern (**Fig.1d**) and the habit of the Na_xIrO_3 crystals (**Fig.1e**).

It is remarkable that intermixing of the Na1 and Ir sites in the stoichiometric Na_2IrO_3 is a common occurrence and accounts for stacking disorder and the distorted honeycomb lattice indicated by two distinct Ir-Ir bond distances, a long one (3.073 Å) and a short one (3.071 Å) [12], both of which are shorter than that in Na_xIrO_3 . In contrast, there is no intermixing of the Na1 and Ir sites in Na_xIrO_3 , giving rise to a perfect honeycomb lattice. However, like those in Na_2IrO_3 [12], the IrO_6 octahedra in Na_xIrO_3 undergo a compression along the c axis. The O-Ir-O bond angle related to the shared edge of the neighboring octahedra is reduced to 80.2° from the undistorted 90° (compared to 84.1° and 84.5° in Na_2IrO_3) and the rest of the O-Ir-O bond angles is increased to 93.4° accordingly (**Fig.1c**). Such a trigonal crystal field could have implications for the splitting of $J_{\text{eff}} = 3/2$ bands [37].

In terms of the oxidation state of Ir in Na_xIrO_3 , for $x = 1$, the Ir ion will be pentavalent Ir^{5+} . However, the average value of x among dozens of the examined crystal samples is around 0.70,

and this gives rise to an average oxidation state of $\text{Ir}^{5.3+}$, a mixed valence state resulting from 70% $\text{Ir}^{5+}(5d^4)$ and 30% $\text{Ir}^{6+}(5d^3)$. The determination of an Ir^{5+} majority in Na_xIrO_3 is also consistent with the following analysis. The Ir-O bond distance, $d_{\text{Ir-O}}$, is 2.028 Å in Na_xIrO_3 , expectedly shorter than 2.188 Å in Na_2IrO_3 with $\text{Ir}^{4+}(5d^5)$; the corresponding ratio of $d_{\text{Ir-O}}(\text{Na}_2\text{IrO}_3)$ to $d_{\text{Ir-O}}(\text{Na}_x\text{IrO}_3)$, $R_{\text{Ir-O}}$, is 1.079. The difference in $d_{\text{Ir-O}}$ is a result of the difference in the ionic radius, r_{Ir} , of Ir, which decreases significantly from 0.625 Å to 0.570 Å to 0.521 Å for Ir^{4+} , Ir^{5+} and Ir^{6+} , respectively, as more electrons are removed from the Ir ion. The ratio of $r_{\text{Ir}^{4+}}$ to $r_{\text{Ir}^{5+}}$ or $R(r_{\text{Ir}^{4+}}/r_{\text{Ir}^{5+}}) = 1.097$ and $r_{\text{Ir}^{4+}}$ to $r_{\text{Ir}^{6+}}$ or $R(r_{\text{Ir}^{4+}}/r_{\text{Ir}^{6+}}) = 1.200$. It is apparent that $R_{\text{Ir-O}} (=1.079)$ is much closer to $R(r_{\text{Ir}^{4+}}/r_{\text{Ir}^{5+}})$ than to $R(r_{\text{Ir}^{4+}}/r_{\text{Ir}^{6+}})$, supporting that Ir is predominately pentavalent Ir^{5+} in Na_xIrO_3 . Unless specified, *all data presented here are those for $x \approx 0.70$.*

It is emphasized that our close examination of single-crystal samples with x ranging from 0.60 to 0.80 indicates that structural and physical properties of Na_xIrO_3 are insensitive to x or Na deficiency [36]. Na_xIrO_3 thus sharply contrasts with another Na-deficient compound, Na_xCoO_2 , in which x varies widely from 0.3 to 0.80 and whose ground state drastically evolves with x [38, 39].

Physical properties Na_xIrO_3 is a Mott insulator. The *ab*-plane electrical resistivity, ρ_{ab} , rises by five orders of magnitude in a manner consistent with a variable-range hopping of carriers between localized states as temperature, T , decreases from 380 K to 25 K (**Fig.2a**).

The low-field magnetization for both the *ab* plane and *c* axis, M_{ab} and M_{c} , exhibits no anomaly in the interval 1.8 K - 350 K at $\mu_0 H = 0.5$ T (**Figs.2b-c**). A Curie-Weiss analysis of the magnetic susceptibility, χ , yields an effective moment, μ_{eff} , of 0.9 and 1.1 μ_{B}/Ir and a Curie-Weiss temperature, θ_{CW} , of -19 and -15 K for the *ab* plane and the *c* axis, respectively (**Fig.2c**; $\Delta\chi = \chi - \chi_0$, with χ_0 the T -independent susceptibility). The values of μ_{eff} are essentially identical to those of the double perovskite antiferromagnets Sr_2YIrO_6 and Ba_2YIrO_6 with pentavalent $\text{Ir}^{5+}(5d^4)$ ions [40,

41]. These values are clearly too large for a singlet $J_{\text{eff}} = 0$ state anticipated for a strong SOI limit in iridates with $\text{Ir}^{5+}(5d^4)$ ions but considerably smaller than $2.83 \mu_B/\text{Ir}$ expected for a spin-only $S = 1$ state without SOI. A reduced value of μ_{eff} is commonplace in iridates, in part because the strong SOI causes a partial cancellation of the spin and orbital contributions [32]. Nevertheless, despite the sizable μ_{eff} and θ_{CW} , no long-range magnetic order occurs above 1.8 K, indicating overwhelming quantum fluctuations in the honeycomb lattice and calling for an examination of the ground state below 1.8 K.

The AC magnetic susceptibility, χ_{ac} , and the heat capacity, $C(T)$, are thus measured down to 0.05 K. χ_{ac} at DC field $H = 0$ displays two peaks denoted by T_h and T_l (red curve in **Fig. 3a**), namely, $T_h = 0.9$ K and $T_l = 0.12$ K for a broad peak and a sharper peak in χ_{ac} , respectively. T_h and T_l track two prominent anomalies observed in $C(T)$ (blue curve, right scale in **Fig. 3a**). $C(T)$ exhibits a broad and yet visible peak near T_h and an abrupt rise at T_l . The entropy removal, ΔS , also shows a slope change near both T_h and T_l , respectively, and a noticeable shoulder situated between T_h and T_l (**Fig. 3b**). ΔS is estimated to be 0.11 J/mole K. This value of ΔS , which is comparable to that for the quantum liquid $\text{Ba}_4\text{Ir}_3\text{O}_{10}$ [42] but much smaller than the $R\ln(3) = 9.12$ J/mole K expected for an $S = 1$ state, implies that Na_xIrO_3 behaves like a Fermi liquid metal where most of the entropy removal happens near a Fermi temperature, T_F , and the T-linear $C(T)$ occurs at $T \ll T_F$.

Indeed, $C(T)$ exhibits a pronounced linear temperature dependence between T_h and T_l or $C(T) = \gamma T$ with an unusually large coefficient $\gamma = 77$ mJ/mole K^2 (**Fig. 3c**). This behavior is anticipated for highly correlated metals and not at all expected for conventional insulators. The linear heat capacity suggests gapless excitations, and the value of γ implies a large residual entropy despite such low temperatures.

For comparison and contrast, $C(T)$ of Na_2IrO_3 is also measured and illustrated along with that of Na_xIrO_3 in **Fig.3c**. The starkly different $C(T)$ of the two sister compounds may help rule out a possible nuclear Schottky anomaly, supporting the unique nature of the upturn marked by T_1 . This point is further strengthened by the corresponding anomaly near T_1 in χ_{ac} . Indeed, a nonlinear behavior of $C(T)$ in a plot of $C(T)$ vs T^{-2} is inconsistent with that of the nuclear Schottky anomaly [Fig.3 in Ref. 36] because the heat capacity of a nuclear Schottky anomaly is expected to scale with T^{-2} . It is also remarkable that $C(T)$ of Na_2IrO_3 (brown curve in **Fig.3c**) monotonically approaches zero with decreasing T due to magnetic entropy removal at $T \leq T_N$. In contrast, $C(T)$ of Na_xIrO_3 (blue curve in **Fig.3c**) is much larger in general and reaches 25 mJ/mole K at T_1 before rising to 68 mJ/mole K at 0.05 K, highlighting strong quantum fluctuations even at sub-Kelvin temperatures.

The characteristic of $C(T)$ for Na_xIrO_3 seems resilient against magnetic fields comparable to the energy scale of T_h and T_1 . As shown in **Figs.4a-b**, the temperature dependence of $C(T)$ changes only slightly at $\mu_0 H = 1$ T but more significantly at $\mu_0 H = 3$ T. The C/T vs T plot in **Fig.4b** illustrates an increasing separation between T_h and T_1 with increasing H . However, application of stronger magnetic field, such as 14 T, suppresses both T_h and T_1 and removes residual entropy, resulting in a behavior consistent with that of a conventional insulator (**Fig.4a**).

Such unusual thermal behavior at sub-Kelvin temperatures clearly contrasts with that of Na_2IrO_3 with $T_N = 18$ K (**Fig.3c**) but bears certain resemblance to that of $(\text{Na}_{1-x}\text{Li}_x)_2\text{IrO}_3$ with $x = 0.80$, at which $T_N = 1.4$ K [15] (**Fig.5a**). This comparison is revealing. An early study of $(\text{Na}_{1-x}\text{Li}_x)_2\text{IrO}_3$ demonstrates that T_N is initially suppressed from 18 K for $x = 0$ to 5 K for $x = 0.28$ and then to 1.2 K for $x = 0.70$ and 1.4 K for $x = 0.80$ before it rises to 7 K for $x = 0.90$ [15] (**Inset in Fig.5b**). Furthermore, the honeycomb structure near $x=0.70$ and 0.80 is least distorted [15], leading

to a speculation that $(\text{Na}_{1-x}\text{Li}_x)_2\text{IrO}_3$ with $x=0.70$ and 0.80 may be closest to the spin liquid [15, 43, 44]. As shown in **Fig.5a**, $C(T)$ at $T > 0.9$ K for both Na_xIrO_3 and $(\text{Na}_{0.2}\text{Li}_{0.8})_2\text{IrO}_3$ behaves in a similar manner, suggesting a similar magnetic nature. However, $C(T)$ for $(\text{Na}_{0.2}\text{Li}_{0.8})_2\text{IrO}_3$ undergoes a rapid decrease below $T_N = 1.4$ K, approaching zero at 0.05 K owing to the magnetic entropy removal; in contrast, $C(T)$ for Na_xIrO_3 decreases less rapidly below $T_h (= 0.9$ K) reaching a minimum of 25 mJ/mole K at T_l before it abruptly rises below T_l (**Fig.5b**). The comparison suggests that T_h may be associated with a short-range order rather than a long-range order because a large residual entropy below T_h remains; T_l marks an onset of strong quantum fluctuations which increases as T approaches absolute zero.

The peculiar heat capacity of Na_xIrO_3 invokes certain theoretical arguments. Theoretical studies of thermal properties for the Kitaev model predict two peaks in the temperature dependence of the specific heat for honeycomb lattices [34, 43, 44]. This two-peak characteristic is a result of fractionalizing a single quantum spin into two types of Majorana fermions, namely, the itinerant Majorana fermion and the localized Majorana fermion. The two peaks in the heat capacity thus correspond to the onset of the thermal excitations or short-range spin correlations of the itinerant Majorana fermions at the high-temperature peak and the thermal excitation of the localized Majorana fermions at the low-temperature peak, respectively [35, 43, 44]. The theoretical studies also anticipate a linear temperature dependence of the heat capacity between the two peaks [43] and a half-plateau-like temperature dependences of the entropy between the two peaks due to the thermal fractionalization of the spin degrees of freedom [44].

It is particularly intriguing that an array of the observed phenomena - the two anomalies marked by T_h and T_l in $C(T)$ (**Fig.3a**), the linearity of $C(T)$ along with the large γ (**Fig.3c**) and the shoulder of ΔS between T_h and T_l (**Fig.3b**) - suggests a strong relevance of Na_xIrO_3 to the

theoretical anticipation for a QSL and an exotic ground state that hosts strong quantum fluctuations coexisting with a short-range spin order. These results along with the comparison with Na_2IrO_3 and $(\text{Na}_{0.2}\text{Li}_{0.8})_2\text{IrO}_3$ inspire a speculation that such a ground state may be in a proximity to the Kitaev spin liquid. Certainly, with a perfect honeycomb lattice and a predominant pseudospin = 1 state Na_xIrO_3 provides a new, perhaps unique candidate material for the search of a Kitaev QSL, which has been elusive to date.

Acknowledgement This work is supported by NSF via grant DMR 1903888.

References

1. A. Kitaev, Anyons in an exactly solved model and beyond. *Ann. Phys.* **321**, 2–111 (2006)
2. G. Jackeli & G. Khaliullin, Mott insulators in the strong spin-orbit coupling limit: from Heisenberg to a quantum compass and Kitaev models. *Phys. Rev. Lett.* **102**, 017205 (2009)
3. J. Chaloupka, G. Jackeli and G. Khaliullin, Kitaev-Heisenberg Model on a Honeycomb Lattice: Possible Exotic Phases in Iridium Oxides A_2IrO_3 , *Phys. Rev. Lett.* **105**, 027204 (2010)
4. C. C. Price and N. B. Perkins, Critical Properties of the Kitaev-Heisenberg Model, *Phys. Rev. Lett.* **109**, 187201 (2012)
5. W. Witczak-Krempa, G. Chen, Y. B. Kim, & L. Balents, Correlated quantum phenomena in the strong spin-orbit regime, *Annu. Rev. Condens. Matter Phys.* **5**, 57–82 (2014)
6. J. G. Rau, E. K.-H. Lee & H.-Y. Kee, Spin-orbit physics giving rise to novel phases in correlated systems: iridates and related materials. *Annu. Rev. Condens. Matter Phys.* **7**, 195 (2016)
7. M. Hermanns, I. Kimchi, & J. Knolle, Physics of the Kitaev model: fractionalization, dynamic correlations, and material connections. *Annu. Rev. Condens. Matter Phys.* **9**, 17 (2018)
8. I. Kimchi, J. P. Sheckelton, T. M. McQueen & P. A. Lee, Scaling and data collapse from local moments in frustrated disordered quantum spin systems. *Nat. Commun.* **9**, 4367 (2018)
9. X. Liu, T. Berlijn, W. G. Yin, W. Ku, A. Tsvelik, Y. J. Kim, H. Gretarsson, Y. Singh, P. Gegenwart and J. P. Hill, Long-range magnetic ordering in Na_2IrO_3 , *Phys. Rev. B* **83**, 220403(R) (2011)
10. F. L. Pratt, P. J. Baker, S. J. Blundell, T. Lancaster, S. Ohira-Kawamura, C. Baines, Y. Shimizu, K. Kanoda, I. Watanabe and G. Saito, Magnetic and non-magnetic phases of a quantum spin liquid, *Nature* **471**, 612 (2011)

11. S. K. Choi, R. Coldea, A. N. Kolmogorov, T. Lancaster, I. I. Mazin, S. J. Blundell, P. G. Radaelli, Y. Singh, P. Gegenwart, K. R. Choi, S. W. Cheong, P. J. Baker, C. Stock and J. Taylor, Spin Waves and Revised Crystal Structure of Honeycomb Iridate Na_2IrO_3 , *Phys. Rev. Lett.* **108**, 127204 (2012)
12. Feng Ye, Songxue Chi, Huibo Cao, Bryan Chakoumakos, Jaime A. Fernandez-Baca, Radu Custelcean, Tongfei Qi, O. B. Korneta, and G. Cao, Direct evidence of a zigzag spin-chain structure in honeycomb lattice: A neutron and x-ray diffraction investigation on single-crystal Na_2IrO_3 , *Phys. Rev. B* **85**, 180403(R) (2012)
13. Y. Singh, S. Manni, J. Reuther, T. Berlijn, R. Thomale, W. Ku, S. Trebst and P. Gegenwart, Relevance of the Heisenberg-Kitaev Model for the Honeycomb Lattice Iridates, *Phys. Rev. Lett.* **108**, 127203 (2012)
14. R. Comin, G. Levy, B. Ludbrook, Z. H. Zhu, C. N. Veenstra, J. A. Rosen, Y. Singh, P. Gegenwart, D. Stricker, J. N. Hancock, D. van der Marel, I. S. Elfimov and A. Damascelli, Na_2IrO_3 as a Novel Relativistic Mott Insulator with a 340-meV Gap, *Phys. Rev. Lett.* **109**, 26 (2012)
15. G. Cao, T. F. Qi, L. Li, J. Terzic, V. S. Cao, S. J. Yuan, M. Tovar, G. Murthy, and R. K. Kaul, Evolution of magnetism in the single-crystal honeycomb iridates $(\text{Na}_{1-x}\text{Li}_x)_2\text{IrO}_3$, *Phys. Rev. B* **88**, 220414(R) (2013)
16. S. Manni, S. Choi, I. I. Mazin, R. Coldea, M. Altmeyer, H. O. Jeschke, R. Valentí, and P. Gegenwart, Effect of isoelectronic doping on the honeycomb-lattice iridate A_2IrO_3 , *Phys. Rev. B* **89**, 245113 (2014)
17. P. Gegenwart and S. Trebst, Kitaev matter, *Nat. Phys.* **11**, 444 (2015)

18. K. A. Modic, T. E. Smidt, I. Kimchi, N. P. Breznay, A. Biffin, S. Choi, R. D. Johnson, R. Coldea, P. Watkins-Curry, G. T. McCandless, J. Y. Chan, F. Gandara, Z. Islam, A. Vishwanath, A. Shekhter, R. D. McDonald and J. G. Analytis, Realization of a three-dimensional spin–anisotropic harmonic honeycomb iridate, *Nat. Commun.* **5**, 4203 (2014)
19. T. Takayama, A. Kato, R. Dinnebier, J. Nuss, H. Kono, L. S. I. Veiga, G. Fabbri, D. Haskel and H. Takagi, Hyperhoneycomb Iridate β -Li₂IrO₃ as a Platform for Kitaev Magnetism, *Phys. Rev. Lett.* **114**, 077202 (2015)
20. S. H. Chun, J. W. Kim, J. Kim, H. Zheng, C. C. Stoumpos, C. D. Malliakas, J. F. Mitchell, K. Mehlawat, Y. Singh, Y. Choi, T. Gog, A. Al-Zein, M. M. Sala, M. Krisch, J. Chaloupka, G. Jackeli, G. Khaliullin and B. J. Kim, Direct evidence for dominant bond-directional interactions in a honeycomb lattice iridate Na₂IrO₃, *Nat. Phys.* **11**, 462 (2015)
21. A. Banerjee, C. Bridges, J.-Q. Yan, A. Aczel, L. Li, M. Stone, G. Granroth, M. Lumsden, Y. Yiu, J. Knolle, S. Bhattacharjee, D. L. Kovrizhin, R. Moessner, D. A. Tennant, D. G. Mandrus & S. E. Nagler, Proximate Kitaev quantum spin liquid behaviour in a honeycomb magnet, *Nat. Mater.* **15**, 733 (2016)
22. S.-H. Baek, S.-H. Do, K.-Y. Choi, Y. S. Kwon, A. U. B. Wolter, S. Nishimoto, J. van den Brink, and B. Büchner, Evidence for a Field-Induced Quantum Spin Liquid in α -RuCl₃ *Phys. Rev. Lett.* **119**, 037201 (2017)
23. J. Zheng, K. Ran, T. Li, J. Wang, P. Wang, B. Liu, Z.-X. Liu, B. Normand, J. Wen, and W. Yu, Gapless Spin Excitations in the Field-Induced Quantum Spin Liquid Phase of α -RuCl₃, *Phys. Rev. Lett.* **119**, 227208 (2017)
24. J. Chaloupka, G. Jackeli, and G. Khaliullin, Zigzag Magnetic Order in the Iridium Oxide Na₂IrO₃, *Phys. Rev. Lett.* **110**, 097204 (2013)

25. R. D. Johnson, S. C. Williams, A. A. Haghighirad, J. Singleton, V. Zapf, P. Manuel, I. I. Mazin, Y. Li, H. O. Jeschke, R. Valentí, and R. Coldea, Monoclinic Crystal Structure of α – RuCl_3 and the Zigzag Antiferromagnetic Ground State, *Phys. Rev. B* **92**, 235119 (2015)
26. H. B. Cao, A. Banerjee, J.-Q. Yan, C. A. Bridges, M. D. Lumsden, D. G. Mandrus, D. A. Tennant, B. C. Chakoumakos, and S. E. Nagler, Low-Temperature Crystal and Magnetic Structure of α - RuCl_3 , *Phys. Rev. B* **93**, 134423 (2016)
27. Ian A. Leahy, Christopher A. Pocs, Peter E. Siegfried, David Graf, S.-H. Do, Kwang-Yong Choi, B. Normand, and Minhyea Lee, Anomalous Thermal Conductivity and Magnetic Torque Response in the Honeycomb Magnet α - RuCl_3 , *Phys. Rev. Lett.* **118**, 187203 (2017)
28. F. Bahrami, W. Lafargue-Dit-Hauret, O. I. Lebedev, R. Movshovich, H.-Y. Yang, D. Broido, X. Rocquefelte, and F. Tafti, Thermodynamic Evidence of Proximity to a Kitaev Spin Liquid in $\text{Ag}_3\text{LiIr}_2\text{O}_6$, *Phys. Rev. Lett.* **123**, 237203 (2019)
29. V. Hermann, M. Altmeyer, J. Ebad-Allah, F. Freund, A. Jesche, A. A. Tsirlin, M. Hanfland, P. Gegenwart, I. I. Mazin, D. I. Khomskii, R. Valentí, and C. A. Kuntscher, Competition between Spin-Orbit Coupling, Magnetism, and Dimerization in the Honeycomb Iridates: α - Li_2IrO_3 under Pressure, *Phys. Rev. B* **97**, 020104 (2018)
30. K. Kitagawa, T. Takayama, Y. Matsumoto, A. Kato, R. Takano, Y. Kishimoto, S. Bette, R. Dinnebier, G. Jackeli & H. Takagi, A spin-orbital-entangled quantum liquid on a honeycomb lattice. *Nature* **554**, 341 (2018)
31. C. Broholm, R. J. Cava, S. A. Kivelson, D. G. Nocera, M. R. Norman, T. Senthil, Quantum spin liquids, *Science* **367**, 263 (2020)
32. Gang Cao and Pedro Schlottmann, The Challenge of Spin-Orbit-Tuned Ground States in Iridates: A Key Issues Review, *Reports on Progress in Physics*, **81** 042502 (2018)

33. J. C. Wang, J. Terzic, T. F. Qi, Feng Ye, S. J. Yuan, S. Aswartham, S. V. Streltsov, D. I. Khomskii, R. K. Kaul and G. Cao, Lattice-Tuned Magnetism of $\text{Ru}^{4+}(4d^4)$ Ions in Single-Crystals of the Layered Honeycomb Ruthenates: Li_2RuO_3 and Na_2RuO_3 , *Phys. Rev. B* **90** 161110 (R) (2014)
34. Changsong Xu, Junsheng Feng, Mitsuaki Kawamura, Youhei Yamaji, Yousra Nahas, Sergei Prokhorenko, Yang Qi, Hongjun Xiang and L. Bellaiche, Possible Kitaev Quantum Spin Liquid State in 2D Materials with $S=3/2$, *Phys. Rev. Lett.* **124**, 087205 (2020)
35. G. M. Sheldrick, Crystal Structure Refinement With SHELXL, *Acta Cryst C* **71**, 1 (2015)
36. Experimental details including the crystal structure of Na_xIrO_3 and measurements
37. H. Gretarsson, J. P. Clancy, X. Liu, J. P. Hill, Emil Bozin, Yogesh Singh, S. Manni, P. Gegenwart, Jungho Kim, A. H. Said, D. Casa, T. Gog, M. H. Upton, Heung-Sik Kim, J. Yu, Vamshi M. Katukuri, L. Hozoi, Jeroen van den Brink, and Young-June Kim, Crystal-Field Splitting and Correlation Effect on the Electronic Structure of A_2IrO_3 , *Phys. Rev. Lett.* **110**, 076402 (2013)
38. Maw Lin Foo, Yayu Wang, Satoshi Watauchi, H.W. Zandbergen, Tao He, R. J. Cava and N. P. Ong, Charge Ordering, Commensurability, and Metallicity in the Phase Diagram of the Layered Na_xCoO_2 , *Phys. Rev. Letts.* **92**, 247001 (2004)
39. L. Viciu, J. W. G. Bos, H. W. Zandbergen, Q. Huang, M. L. Foo, S. Ishiwata, A. P. Ramirez, M. Lee, N. P. Ong and R. J. Cava, Crystal structure and elementary properties of Na_xCoO_2 ($x=0.32, 0.51, 0.6, 0.75$, and 0.92) in the three-layer NaCoO_2 family, *Phys. Rev. B* **73**, 17410 (2006)
40. G. Cao, T. F. Qi, L. Li, J. Terzic, S. J. Yuan, L. E. DeLong, G. Murthy and R. K. Kaul, Novel magnetism of $\text{Ir}^{5+}(5d^4)$ ions in the double perovskite Sr_2YIrO_6 , *Phys. Rev. Lett.* **112**, 056402 (2014)

41. J. Terzic, H. Zhang, Feng Ye, P. Schlottmann, H. D. Zhao, L. DeLong, S. J. Yuan and G. Cao, Evidence for a magnetic state in double-perovskite iridates with $\text{Ir}^{5+}(5d^4)$ ions, *Phys. Rev. B* **96**, 064436 (2017)
42. G. Cao, H. D. Zhao, H. Zheng, Y. Ni, C. A. Pocs, Y. Zhang, F. Ye, C. Hoffmann, X. Wang, M. Lee, M. Hermele and I. Kimchi, Quantum liquid from strange frustration in the trimer magnet $\text{Ba}_4\text{Ir}_3\text{O}_{10}$, *npj Quantum Materials* **5**, 26 (2020)
43. J. Nasu, M. Udagawa, and Y. Motome, Thermal fractionalization of quantum spins in a Kitaev model: Temperature-linear specific heat and coherent transport of Majorana fermions, *Phys. Rev. B* **92**, 115122 (2015)
44. Y. Yamaji, T. Suzuki, T. Yamada, S.-I. Suga, N. Kawashima, and M. Imada, Clues and criteria for designing a Kitaev spin liquid revealed by thermal and spin excitations of the honeycomb iridate Na_2IrO_3 , *Phys. Rev. B* **93**, 174425 (2016)
45. K. Momma and F. Izumi, VESTA 3 for three-dimensional visualization of crystal, volumetric and morphology data, *J. Appl. Crystallogr.*, **44**, 1272-1276 (2011)

Captions

Fig.1. Crystal Structure of Na_xIrO_3 : (a) the ab plane, (b) ab planes stacking along the c axis, (c) the honeycomb ring formed by edge-sharing IrO_6 octahedra (the values are for $x=0.73$), (d) a snapshot of the X-ray diffraction pattern showing the honeycomb lattice and (e) a single-crystal sample with a hexagon. Note that VESTA [45], a virtualization program for crystal structures used here, yields mixed colors of both yellow and white for Na1 sites within the honeycomb rings to indicate the Na deficiency and a single color of yellow for Na2 sites to illustrate the full occupancy. More importantly, all Ir-Ir bond distances in the honeycomb ring are equal, giving rise to a robust, undistorted honeycomb lattice, regardless Na vacancies at the Na1 sites.

Fig.2. Transport and Magnetic Properties of Na_xIrO_3 : The temperature dependence of (a) the ab -plane resistivity ρ_{ab} , (b) the magnetization for the ab plane and c axis, M_{ab} and M_c , and (c) the reciprocal magnetic susceptibility for the ab plane and c axis $\Delta\chi_{ab}^{-1}$ and $\Delta\chi_c^{-1}$. **Inset in (b):** M_{ab} and M_c vs $\log T$ for clarification.

Fig.3. AC Susceptibility and thermal properties of Na_xIrO_3 : The temperature dependence of (a) the AC susceptibility χ_{ac} (red curve) at 10 kHz and an AC field $H_{ac} = 3.1$ Oe, and heat capacity $C(T)$ (blue curve, right scale), (b) the entropy removal ΔS and (c) $C(T)$ for both Na_xIrO_3 and Na_2IrO_3 for comparison. Note that the yellow oval in (a) outlines the broad peak near T_h and the red dashed lines in (b) and (c) are a guide to the eye, highlighting the linearity of the region between T_h and T_l .

Fig.4. Heat Capacity of Na_xIrO_3 : The temperature dependence of (a) $C(T)$ and (b) C/T at a few representative magnetic fields applied along the c axis.

Fig.5. Heat Capacity of Na_xIrO_3 and $(\text{Na}_{0.2}\text{Li}_{0.8})_2\text{IrO}_3$ for comparison: The temperature dependence of **(a)** $C(T)$ and **(b)** C/T . **Inset in (a):** the ab -plane magnetic susceptibility χ_a for $(\text{Na}_{0.2}\text{Li}_{0.8})_2\text{IrO}_3$; **Inset in (b):** T_N as a function of Li concentration x . Note that $T_N = 1.4$ K at $x=0.80$ of Li doping where the honeycomb lattice is nearly undistorted [15].

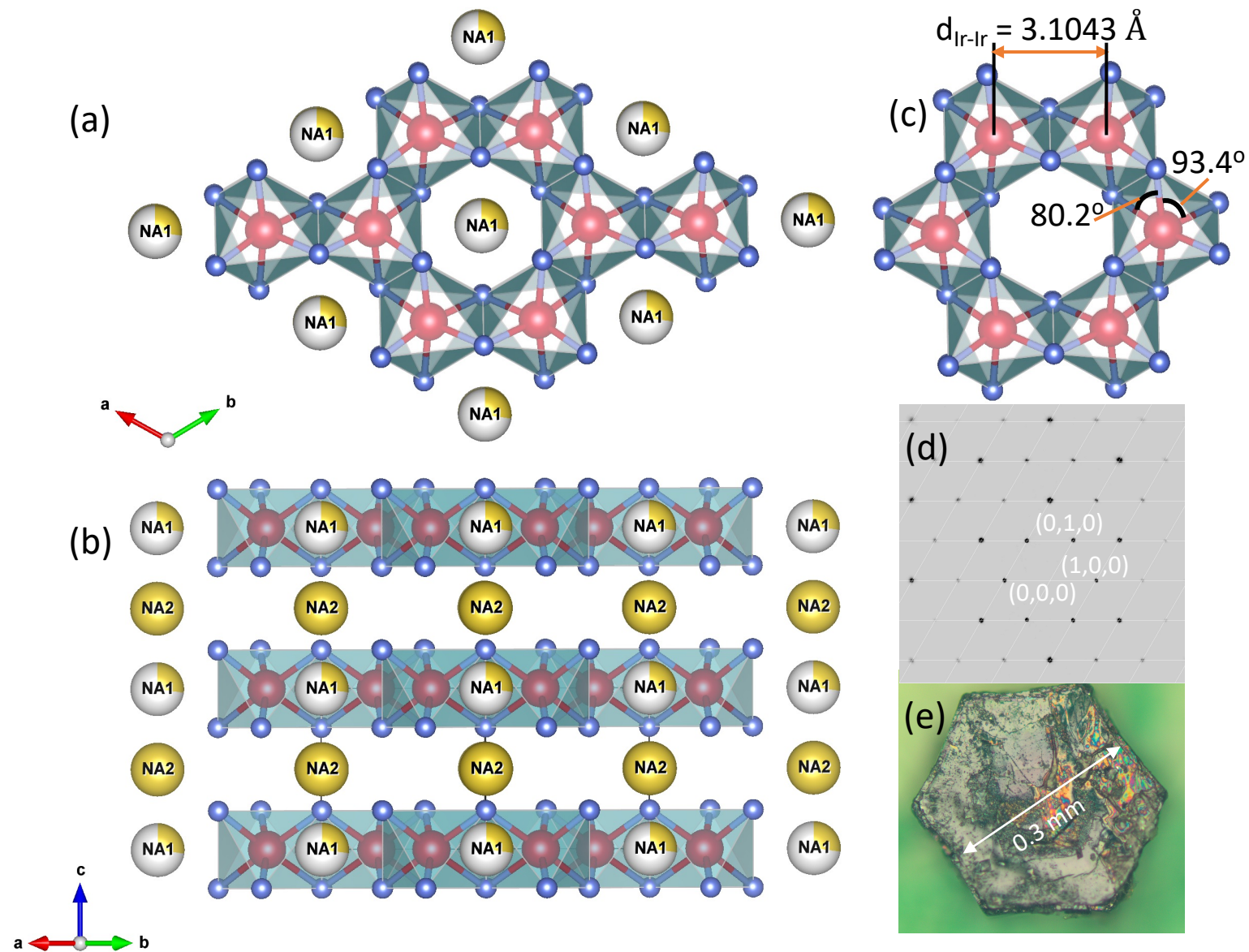


Figure 1

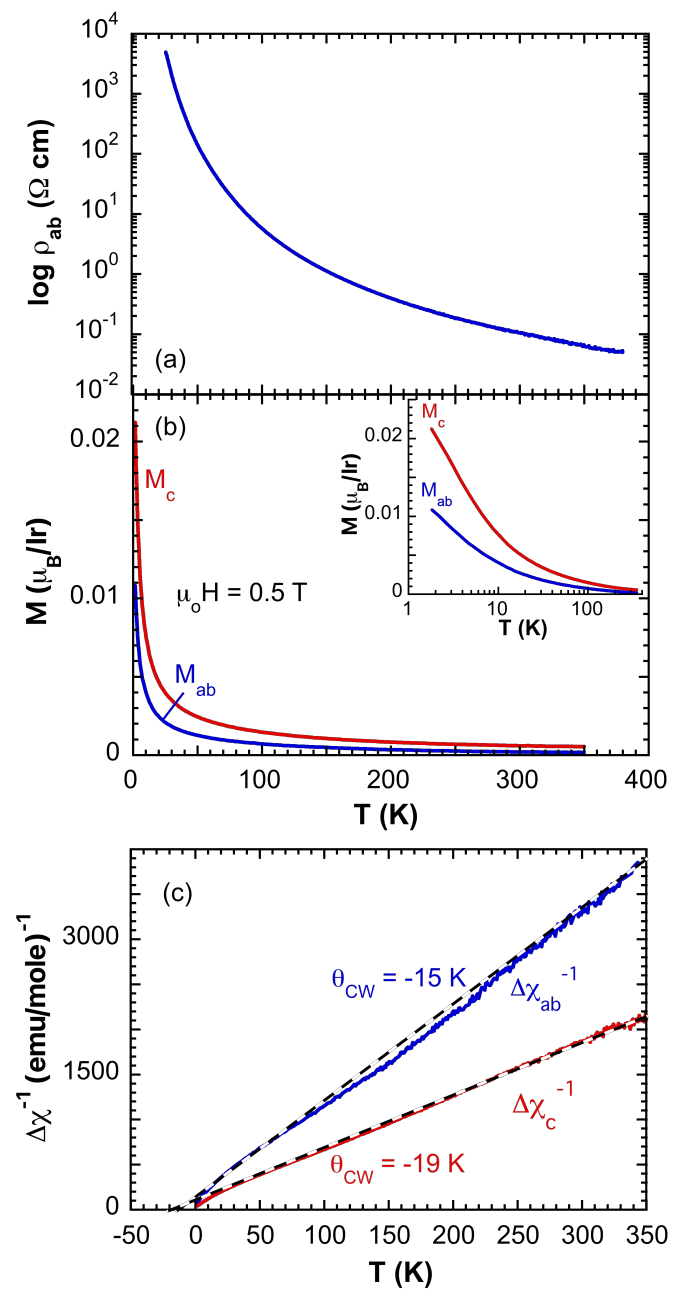


Figure 2

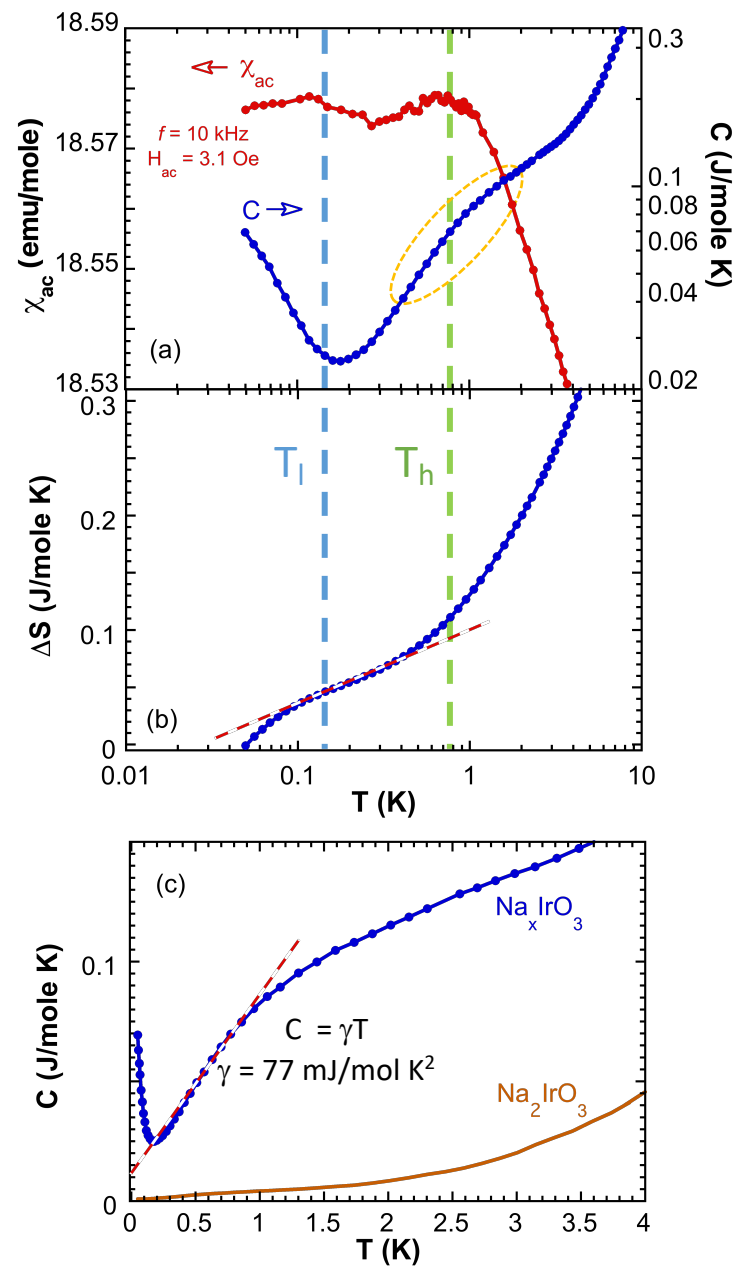


Figure 3

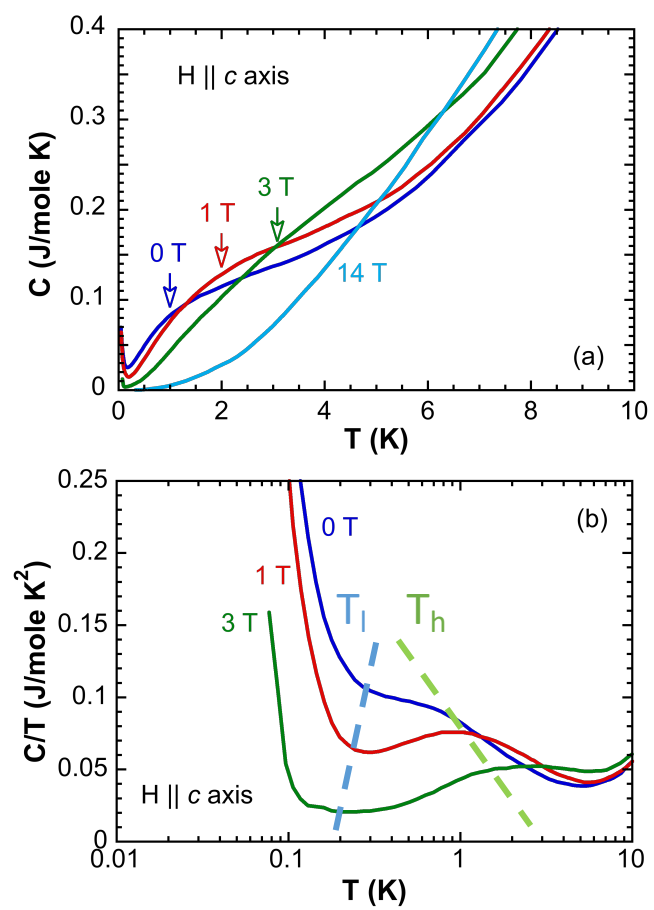


Figure 4

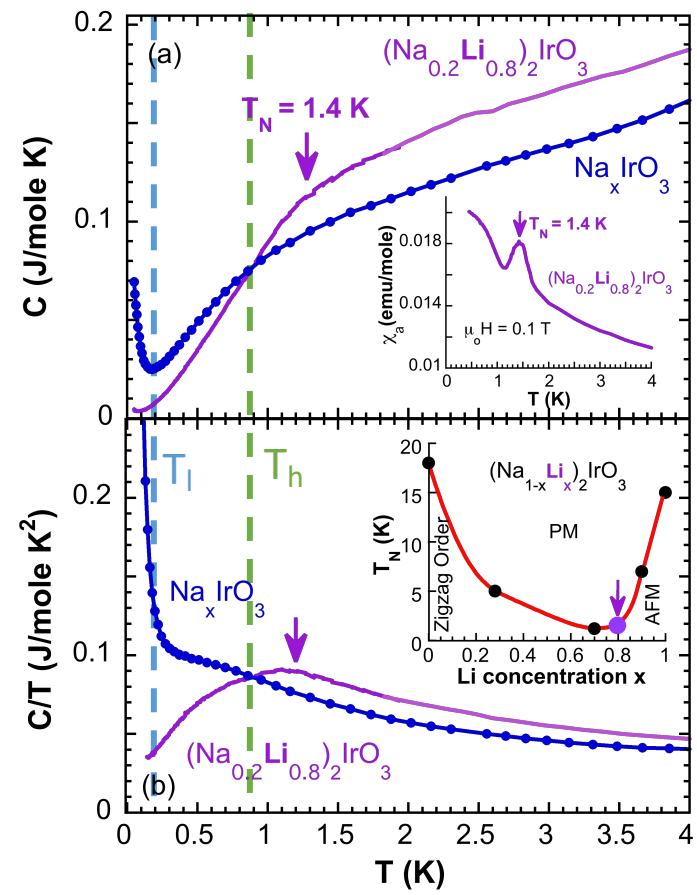


Figure 5